Noise induced escape from a nonhyperbolic chaotic attractor of a periodically driven nonlinear oscillator

Zhen Chen, Yang Li, and Xianbin Liu

Citation: Chaos **26**, 063112 (2016); doi: 10.1063/1.4954028
View online: http://dx.doi.org/10.1063/1.4954028
View Table of Contents: http://scitation.aip.org/content/aip/journal/chaos/26/6?ver=pdfcov
Published by the AIP Publishing

Noise induced escape from a nonhyperbolic chaotic attractor of a periodically driven nonlinear oscillator

Zhen Chen,[a] Yang Li, and Xianbin Liu[a]
State Key Lab of Mechanics and Control for Mechanical Structures, College of Aerospace Engineering, Nanjing University of Aeronautics and Astronautics, 29 Yudao Street, Nanjing 210016, People's Republic of China

(Received 29 February 2016; accepted 3 June 2016; published online 16 June 2016)

Noise induced escape from the domain of attraction of a nonhyperbolic chaotic attractor in a periodically excited nonlinear oscillator is investigated. The general mechanism of the escape in the weak noise limit is studied in the continuous case, and the fluctuational path is obtained by statistical analysis. Selecting the primary homoclinic tangency as the initial condition, the action plot is presented by parametrizing the set of escape trajectories and the global minimum gives rise to the optimal path. Results of both methods show good agreements. The entire process of escape is discussed in detail step by step using the fluctuational force. A structure of hierarchical heteroclinic crossings of stable and unstable manifolds of saddle cycles is found, and the escape is observed to take place through successive jumps through this deterministic hierarchical structure. *Published by AIP Publishing*. [http://dx.doi.org/10.1063/1.4954028]

Noise induced escape plays a fundamental role in a broad range of processes and has been extensively studied in recent years. This paper investigated the noise induced escape from a nonhyperbolic chaotic attractor of a periodically excited nonlinear oscillator and uncovered the general mechanism of the escaping process. We demonstrate in this work that in weak noise limit the escape follows certain path with overwhelming probability and such path is unique. With respect to the structure of nonhyperbolic attractor, it is shown that escaping process initiates at some special point of the attractor's fractal structure, which turns out to be the primary homoclinic tangency (PHT). Uncovering such mechanism allows us to consider topological properties and singularities, such as cusps and caustics, of the pattern of escaping paths from a chaotic attractor. These results shed new light on the problem of noised induced escape from a chaotic attractor and make further studies of patterns and singular features possible.

I. INTRODUCTION

The consideration of random perturbations extends the notion of perturbations in deterministic cases, making allowance of the fact that instead of absolute smallness for all time it may be assumed that the perturbations are small only in mean over the ensemble of all possible realizations. Small random perturbations may assume large values, but the probability of these large values is small. Such an extension leads to effects not characteristic of small deterministic perturbations. Especially intriguing new features occur when considering a long lasting effect of small random perturbations. One of them is large fluctuations occurring only rarely but responsible for many physical processes,[1–4] or noised-induced escape related to the stability of attractors in the presence of weak noise.

In the past two decades, a great deal of mathematical and experimental effort has been devoted to the study of large fluctuations in nonequilibrium systems,[5–8] using Hamiltonian formalism[9] or equivalent path integral formulations.[10–12] The method is based on the concept of optimal paths along which the system fluctuates to a remote state with overwhelming probability. Through a proper formulation of a statistical distribution function, i.e., prehistory probability distribution,[5,13] experimental approaches by means of analogue electronic circuits[14,15] were proposed to prove the physical existence of such paths. The mathematical foundation of these concepts involves a set of dynamical equations providing extremums of certain action functional in the path integral formulation of the stochastic process. The optimal path gives rise to the absolute minimum to the action functional which characterizes the difficulty of the arrival at a given point along different paths. The quantity of the action serves as the exponential rate of a stationary probability density in approximated WKB form in the weak noise limit.[16] As noise intensity tends to zero, these probabilities become exponentially small but the rate of falling off is path dependent. It follows that for a given noise intensity, the probability for the system moving along the optimal path is exponentially larger than ones of motions along other paths. We remark that extreme paths provide local extremums to the action functional, rather than global minimum. Patterns of extreme paths for nonequilibrium systems may have singular features.[17–19] Variational equations to calculate optimal paths are well known both for continuous and discrete systems,[16] but methods of solving them have only been proposed for special cases of escaping from fixed points or limit cycles.[18,20]

[a]Authors to whom correspondence should be addressed. Electronic addresses: czkillua@icloud.com and xbliu@nuaa.edu.cn. Tel./Fax: +86-25-84892106.

In particular, noise-induced escape from a chaotic attractor plays an extremely significant role in the theory of fluctuations whose applications include laser system, neuron dynamics, and the control of migration in multi-stable systems. However, solving such problems is a formidable task as a result of the complicated structures of a chaotic attractor and the obscureness of the way in which a fluctuational trajectory breaks away. Limited work has been done in this field using the Hamiltonian theory of large fluctuations. Anishchenko *et al.*[21,22] studied the noised induced escape from a quasi-hyperbolic attractor in the Lorenz system, showing that there exists a unique escape path consisting of three parts and the role of noise in each part is different. Noise induced escape from a nonhyperbolic chaotic attractor in a periodically excited nonlinear oscillator was considered by Luchinskii and Khovanov[23] via a statistical analysis of the escaping paths. The same system was studied in terms of the energy optimal control of chaos,[24] connecting the Wentzel-Freidlin Hamiltonian in the analysis of fluctuations with Pontryagin's Hamiltonian in the control problem. According to Suso and Celso,[25] escape from a nonhyperbolic chaotic attractor starts at the primary homoclinic tangency[26] closest to the basin boundary. Their findings were substantiated in the discrete case with the help of Hénon and Ikeda map.

The main purpose of this paper is to uncover the same mechanism of escape from a nonhyperbolic chaotic attractor in a continuous system driven by weak white nose. In Ref. 24, an unstable periodic orbit embedded in the chaotic attractor was identified by an inspection of ridges of the distribution of escape paths and taken as the initial condition of the optimal path. However, in this paper, an unstable periodic orbit was first acquired by the generalized cell mapping with digraph (GCMD) method, completely not involved with escape scenario. Then numerically and theoretically, we show that escape just starts from this unstable periodic orbit and furthermore, in a Poincaré section the point where escape begins turns out to be the primary homoclinic tangency of the chaotic attractor.

This paper is organized as follows. In Section II, we formulate the problem and give some ranges of parameters appearing in the system. Global analysis of the system by GCMD method is performed in Section III and subsequently in Section IV Hamiltonian formalism is employed, leading to an auxiliary dynamical system. Statistical analysis using the concept of prehistory probability distribution is presented in Section V, giving rise to the fluctuational path. It is testified with the one corresponding to the global minimum of the action plot and they show rather good agreement in Section V. In Section VI, we give the results of primary homoclinic tangency and the action plot. In Section VII, we investigate the whole process of escape and study each step with the help of fluctuational force. The escaping mechanism is discussed. The results are discussed and summarized in Section VIII with conclusions drawn.

II. FORMULATION

A periodically excited nonlinear oscillator in the presence of noise was chosen as the model for investigation

$$\begin{aligned}\dot{q}_1 &= K_1(\mathbf{q}(t)) = q_2\\ \dot{q}_2 &= K_2(\mathbf{q}(t)) = -2\Gamma q_2 - \omega_0^2 q_1\\ &= -\beta q_1^2 - \gamma q_1^3 + h\sin(\omega_f t) + \xi(t).\end{aligned} \tag{1}$$

Here, q_1, q_2 are dynamical variables and $\xi(t)$ is the Gaussian White noise such that $\langle\xi(t)\rangle = 0$, $\langle\xi(t)\xi(0)\rangle = D\delta(t)$. D is the noise intensity. $\Gamma, \omega_0, \beta, \gamma, h, \omega_f$ are parameters, which are chosen such that the potential is monostable ($\beta < 4\gamma\omega_0^2$) and the dependence of the energy of oscillations on their frequency is nonmonotonic ($\beta^2/\gamma\omega_0 > 9/10$). The motion is underdamped ($\Gamma \le \omega_f \approx 2\omega_0$), and chaos could occur for a relatively small periodic force amplitude $h \approx 0.1$, as shown previously.[24] This model has considerable appeal for researchers in a number of contexts since theoretical analysis can be performed for an extensive range of parameters.[27]

A bifurcation diagram for (1) in Poincaré section with $\omega_f t = 0(\mathrm{mod}\, 2\pi)$ is illustrated in Fig. 1(a) for certain parameters $(\Gamma = 0.025,\ \omega_0 = 0.597, \beta = 1, \gamma = 1, \omega_f = 1.005)$, which will be used throughout this paper. As can be seen, the region of the large stable limit cycle of period 1 (SC1) locates between arrows 1 and 3 and the coexistence of the chaotic attractor lies between arrows 2 and 3. The chaotic attractor emerges as the result of periodic-doubling bifurcations, and thus corresponds to a nonhyperbolic attractor (NHA). These are seen much more clearly in Fig. 1(b), which shows an enlargement of Fig. 1(a) in the range of 0.13–0.144.

III. GLOBAL ANALYSIS OF DETERMINISTIC DYNAMICS

To begin with, global properties of Eq. (1) without noise are studied by the generalized cell mapping with digraph (GCMD) method.[28] Among all global properties, the most important one is probably the set of all the attractors representing the long-term steady motions. In this context, the attractors are the SC1 and the NHA. In addition, one is also interested in locating the domain of attraction for each attractor and the boundary sets between them. Besides that, the GCMD method could also determine the unstable invariant sets in the state space, such as saddles and chaotic saddles. The basic idea of this approach is the primitive notion that a dynamical system is actually an ordering machine which assigns the fore-and after relations between points of phase space. In the GCMD method, a small region whose size can be made arbitrarily small, referred to as a cell, is used to represent points in it. Consequently, the system is put in their discretized forms and the ordering between original points is replaced by the ordering between cells. An essential concept of self-cycling sets of the graph theory is also employed to decide attractors or other invariant sets. For more details, one can refer to Ref. 29.

The coexisting NHA and SC1 are shown in Fig. 2(a) for the same Poincaré cross-section as Fig. 1 in the absence of noise. We take the case $h = 0.143$ for consideration. There exist a saddle cycle of period 3 (UC3) around the NHA, indicated by black circles and a saddle cycle of period 1 (UC1), shown by black squares. The domain of attraction of NHA

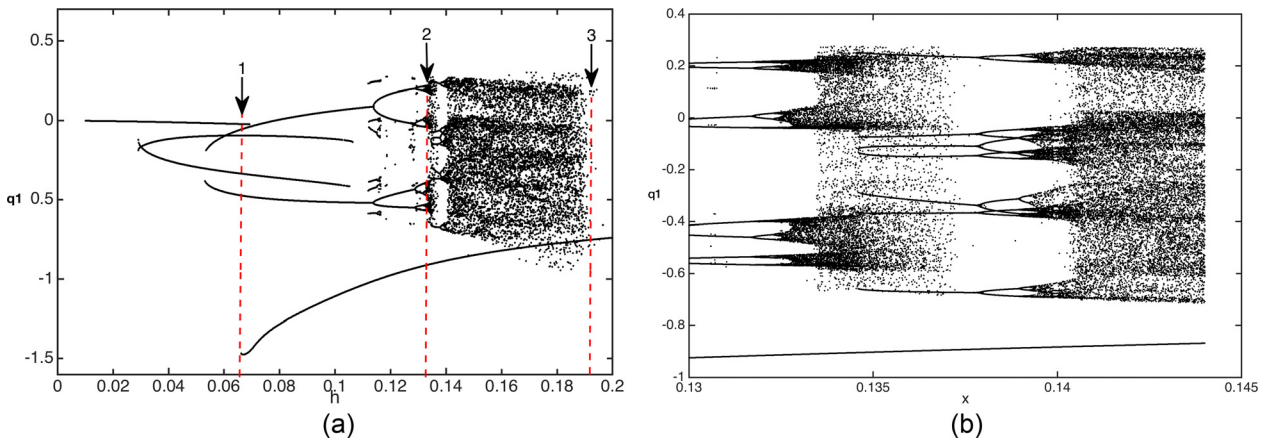

FIG. 1. (a) A bifurcation diagram for (1) in Poincaré section obtained with $\omega_f t = 0\,(mod\,2\pi)$, $\omega_f = 1.005$ shows the component of q_1 for different h. The region of existence of SC1 lies between arrows 1 and 3. The region of coexistence of a chaotic attractor lie between arrows 2 and 3. (b) A local amplification of the interval of h ranging from 0.13 to 0.144.

(shaded) and domain of attraction of SC1 (white) are shown in Fig. 2(b). It is observed that the boundary of attraction of NHA is not fractal and is formed by the stable invariant manifold of UC1, depicted by magenta curves. The green curves in Fig. 2(b) correspond to the unstable manifold of UC1, leading to SC1 in one direction and NHA in the other direction.

One may question the existence of the unstable cycles since they appear as collections of points, as shown in Fig. 2(a). This can be judged by dividing the whole phase space into more cells, that is to say, making the size of a cell smaller and the approximation to original system more accurate. The division in Fig. 2 is 300×300. Finer divisions of the phase space can be made but it is quite time-consuming. However, we can construct a second-level cell state space by subdividing cells of interest only, such as the original cells of UC3 or UC1. Then the same procedure of GCMD is carried out to the second-level cell state space. If the original unstable cycle does exist, it still persists as a self-cycle set in this procedure. Or it would not survive under refining. This is an iterative method introduced by Hsu.[29] This iterative procedure can be repeated to refine a self-cycle set to any degree of accuracy we desire. We show some of the results in Fig. 3 below.

We first take 200×200 cells to cover $-1 \le x \le 0.5$ and $-1 \le y \le 0.5$ with the cell size at the first level being 0.0075×0.0075, as shown in Fig. 3(a). It is seen that UC3 consists of a number of cells occupying a large area. The second level cell state space is then constructed within original cells of UC1, UC3 and also NHA to disclose its finer structure. Letting a cell be divided into 3×3 smaller cells we obtain Fig. 3(b), of which the cell size is 0.0025×0.0025. The area of UC3 clearly decreases and NHA shows more details. Repeat this refining process by taking more subcells

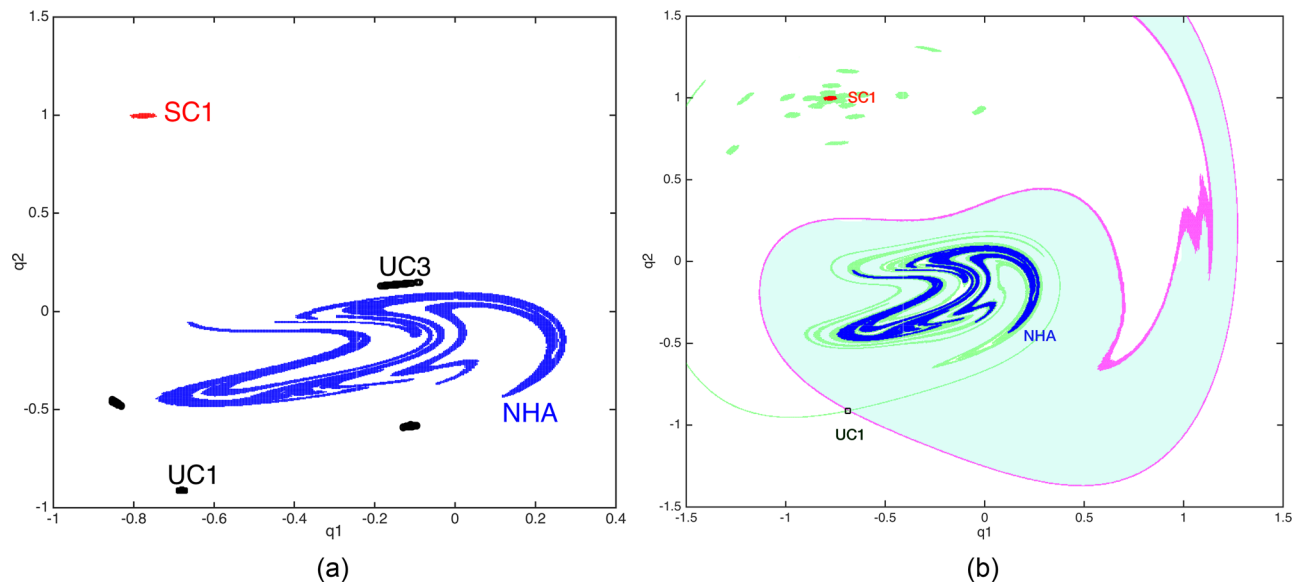

FIG. 2. (a) Attractors and unstable periodic states of (1) in the absence of noise in Poincaré section $\omega_f t = 0\,(\mathrm{mod}\,2\pi)$, $\omega_f = 1.005$. We take other parameters as $\Gamma = 0.025$, $\omega_0 = 0.597$, $\beta = 1$, $\gamma = 1$, $h = 0.143$. A cell space of 300×300 is used to cover $-1.5 \le x \le 1.5$ and $-1.5 \le y \le 1.5$. The cell size is 0.005×0.005. (b) The basin of attraction of NHA indicated by cyan shaded regions. The magenta curves are the stable manifolds of UC1, and green curves are its unstable manifolds (the UC3 is omitted for clarity).

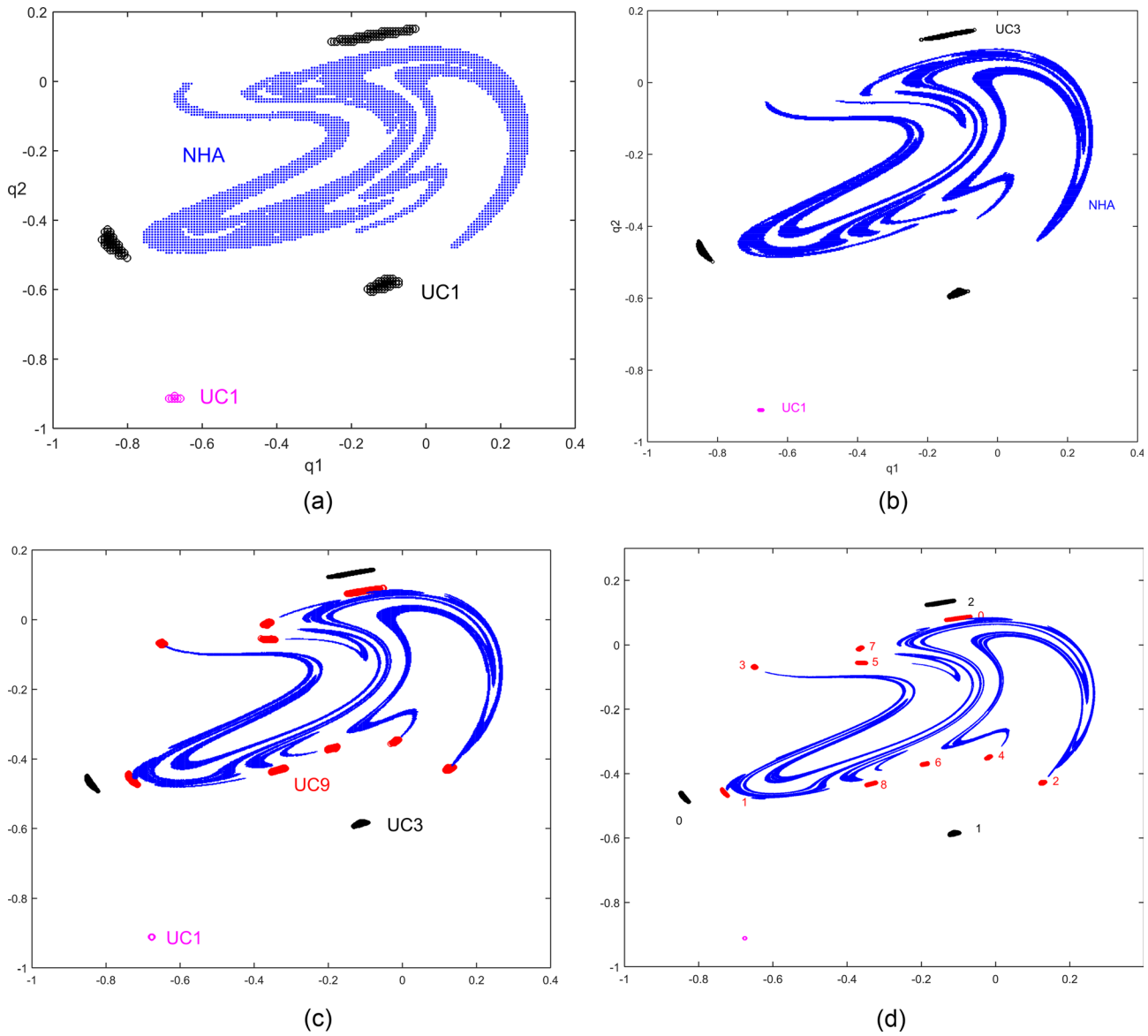

FIG. 3. (a). The first level state space of 200 × 200 cells, with the cell size being 0.0075 × 0.0075. Black circles represent unstable cycles, and the blue dots represent NHA. (b) The second level state space by dividing each cell in (a) into 3 × 3 smaller cells, with the cell size being 0.0025 × 0.0025. (c) Divide each cell in (a) into 4 × 4 cells and the cell size is 0.001875 × 0.001875. (d) Divide each cell in (a) into 8 × 8 cells and the cell size is 0.0009375 × 0.0009375.

in each cell of the first level, and results are presented in Figs. 3(c) and 3(d). It is found that the UC3 and UC1 do persist under refining and moreover, in the close neighborhood of NHA there exists an unstable saddle cycle of period 9 (UC9) indicated by red circles with numbers 0–8 to reveal the order of iteration in Fig. 3(d). To make it more precise, if one starts at point-0 it will be mapped into point-1, point-2,…, point-8, and then back to point-0 again. We will explain the role which these unstable saddle cycles play in the process of escape in more detail later.

IV. THEORETICAL ANALYSIS OF NONEQUILIBRIUM FLUCTUATIONAL TRANSITIONS

Up to now we have studied global dynamics of the deterministic form of Eq. (1) such as attractors, domains of attraction, and boundary sets. We are now in a position to consider large fluctuations in the domain of attraction of NHA. If the noise intensity D is small, the system spends most of the time fluctuating about the attractor, only occasionally far away from it (of scale $\gg \sqrt{D}$). Furthermore, escape from the domain of attraction could occur. When it does occur, escape follows a unique optimal trajectory with overwhelming probability, seemingly in an almost deterministic way. To determine the optimal trajectory, we must turn to investigate the asymptotic solution of the Fokker-Planck equation for Eq. (1) as $D \to 0$, which is

$$\frac{D}{2}\frac{\partial^2}{\partial q_i \partial q_j}\left[Q_{ij}P(\boldsymbol{q})\right] - \frac{\partial}{\partial q_i}\left[K_i(\boldsymbol{q})P(\boldsymbol{q})\right] = 0. \tag{2}$$

The matrix $Q_{ij} = \delta_{i2}\delta_{j2}$ and $P(\boldsymbol{q})$ is the stationary probability density. In the limit of weak noise intensity D, one can seek an approximate solution of Eq. (2) in an eikonal or WKB form

$$P(\boldsymbol{q}) \sim C(\boldsymbol{q}) \exp\left[-S(\boldsymbol{q})/D\right] \tag{3}$$

with $C(\boldsymbol{q})$ being a prefactor not investigated in this paper and $S(\boldsymbol{q})$ being the "activation energy" of fluctuations to the vicinity of the point $\boldsymbol{q}$ in the state space.[22] $S(\boldsymbol{q})$ is also called quasipotential or nonequilibrium potential.[30]

Substituting Eq. (3) into Eq. (2) and keeping only the terms of lowest order in D, we obtain the Hamilton–Jacobi equation for $S(\boldsymbol{q})$

$$H(\boldsymbol{q},\boldsymbol{p}) \equiv \boldsymbol{K}(\boldsymbol{q})\cdot\boldsymbol{p} + \frac{1}{2}\boldsymbol{p}^T\boldsymbol{Q}\boldsymbol{p} = 0, \quad \boldsymbol{p} \equiv \frac{\partial S}{\partial \boldsymbol{q}}, \tag{4}$$

where the matrix $\boldsymbol{Q}$ and $\boldsymbol{K}$ correspond to Q_{ij} and K_i in Eq. (2), respectively. To solve the Hamilton-Jacobi equation (4), one can employ the method of characteristics, arriving at the following equations:

$$\begin{aligned} \frac{d\boldsymbol{q}}{dt} &= \frac{\partial H}{\partial \boldsymbol{p}} = \boldsymbol{K}(\boldsymbol{q}) + \boldsymbol{Q}\boldsymbol{p}, \\ \frac{d\boldsymbol{p}}{dt} &= -\frac{\partial H}{\partial \boldsymbol{q}} = -\left[\frac{\partial \boldsymbol{K}(\boldsymbol{q})}{\partial \boldsymbol{q}}\right]^T \boldsymbol{p}, \end{aligned} \tag{5}$$

and the evolution equation for S along any characteristic is

$$\frac{dS}{dt} = \boldsymbol{p}\cdot\dot{\boldsymbol{q}}. \tag{6}$$

Note that Eq. (5) leads to an auxiliary Hamiltonian dynamical system, with the Wenzel-Freidlin Hamiltonian $H(\boldsymbol{q},\boldsymbol{p})$. From this point of view, $S(\boldsymbol{q})$ can be interpreted as the classical action at zero energy.[18]

Solutions of Eq. (5) describe trajectories yielding extreme values of the cost functional[24] of the form

$$\mathrm{S}[\boldsymbol{q}(t)] = \frac{1}{2}\int_{t_0}^{t_f} \xi^2(t)dt, \tag{7}$$

with $\boldsymbol{q}(t)$ being certain trajectory driven by the corresponding realization of $\xi(t)$ and satisfying $\boldsymbol{q}(t_0) = \boldsymbol{q}_0$ and $\boldsymbol{q}(t_f) = \boldsymbol{q}_f$. Since using (1) the cost functional (7) can be transformed into an action functional

$$S[\mathbf{q}(\mathrm{t})] = \int_{t_0}^{t_f} dt\, L(\boldsymbol{q},\dot{\boldsymbol{q}}), \quad \mathrm{L}(\mathbf{q},\dot{\mathbf{q}}) = \frac{1}{2}(\dot{\boldsymbol{q}} - \boldsymbol{K})^T(\dot{\boldsymbol{q}} - \boldsymbol{K}). \tag{8}$$

This has the form of a Lagrangian L for a classical mechanical system. As $\mathrm{D} \to 0$, these path integrals (8) can be evaluated by means of steepest descents and the paths dominating the integrals are the ones giving rise to $\frac{\delta S}{\delta x} = 0$. This results in a Euler-Poisson equation for extreme paths, which is a 2nth-order nonlinear partial differential equation and through applying the following relations:[9]

$$p_i = \sum_{j=1}^{n} (-1)^{j-i} \frac{d^{j-i}}{dt^{j-i}}\left(\frac{\partial L}{\partial q^{(j)}}\right), \tag{9}$$

$$L = \sum_i p_i\dot{q}_i - H, \tag{10}$$

it can be converted into 2n first-order ordinary differential equation (5). In other words, the action $S(\boldsymbol{q})$ mentioned above is just given by the variational problem of (8). Combining (1) and formulas (8)–(10), we have the following:

$$\begin{aligned} S(q_1,t) &= \int_{t_0}^{t_f} dt\, L(q_1,\dot{q}_1,\ddot{q}_1,t), \\ L(q_1,\dot{q}_1,\ddot{q}_1,t) &= \frac{1}{2}\left[\ddot{q}_1 + 2\Gamma\dot{q}_1 + \omega_0^2 q_1 + \beta {q_1}^2 \right. \\ &\quad \left. + \gamma {q_1}^3 + h\sin(\omega t)\right], \end{aligned} \tag{11}$$

and the so-called Wenzel-Freidlin Hamiltonian for (1)

$$\begin{aligned} H &= \frac{1}{2}p_2^2 + p_1 q_2 + \left(-2\Gamma q_2 - \omega_0^2 q_1 - \beta {q_1}^2 \right. \\ &\quad \left. - \gamma {q_1}^3 - h\sin(\omega_f t)\right)p_2, \\ p_i &= \frac{\partial S}{\partial q_i},\ i = 1,2. \end{aligned} \tag{12}$$

Hence Eq. (5) for system (1) is a four dimensional Hamiltonian system as follows:

$$\begin{aligned} \dot{q}_1 &= \dot{q}_2 \\ \dot{q}_2 &= p_2 - 2\Gamma q_2 - {\omega_0}^2 q_1 - \beta {q_1}^2 - \gamma {q_1}^3 + h\sin(\omega_f t), \\ \dot{p}_1 &= ({\omega_0}^2 + 2\beta q_1 + 3\gamma {q_1}^2)p_2, \\ \dot{p}_2 &= -p_1 + 2\Gamma p_2. \end{aligned} \tag{13}$$

In general, there will be many extreme trajectories of (13) starting from initial state $\boldsymbol{q}_0$ to final state $\boldsymbol{q}_f$, thus the action $S(\boldsymbol{q}_f)$ is multivalued. Only least action path corresponds to the physical realization of the noise. Taking all such realizations $\xi(t)$ into consideration, there exists one giving the least action. This least action $S_{min}(\boldsymbol{q}_f)$ is the actual value that appears in the WKB approximation (3) and the corresponding $\boldsymbol{q}(t)$ is the optimal trajectory $\boldsymbol{q}_{opt}(t)$. We finally remark that the multivaluedness of the action S may bring singularities of topology of the manifold traced by extreme trajectories.

V. STATISTICAL ANALYSIS OF NONEQUILIBRIUM FLUCTUATIONAL TRANSITIONS

According to Sec. IV, it can be easily seen that optimal paths play a crucial role in the whole theory. However, there is no general method to solve Eq. (2) analytically for nonequilibrium system. Then we have to resort to some approximate methods, one of which is the concept of prehistory probability distribution $P_h(\boldsymbol{q},t|\boldsymbol{q}_f,t_f)$, first proposed by Dykman *et al.*[5] It turns out to be an appropriate statistical method to describe the distribution of fluctuational paths, both theoretically and experimentally.[14] By definition, $P_h(\boldsymbol{q},t|\boldsymbol{q}_f,t_f)$ is given by a ratio of the three-time transition probability $P(\boldsymbol{q}_f,t_f|\boldsymbol{q},t;\boldsymbol{q}_i,t_i)$ to the two-time one $P(\boldsymbol{q}_f,t_f|\boldsymbol{q}_i,t_i)$, with the initial instant of time t_i having been set equal to $-\infty$ so that both t_i and $\boldsymbol{q}_i$ have dropped out from P_h. This distribution contains all the information on the temporal evolution of the system before arriving at $\boldsymbol{q}_f$. The existence of an optimal path of escape from the attractor can be confirmed by the shape of P_h. Due to the fact that optimal paths are ones along which the system moves during escape with overwhelming probability, the prehistory

probability distribution peaks sharply around the optimal path as $D \to 0$. Thus when experimentally studying P_h, one could find a region in the phase space with which the optimal path is clearly seen, i.e., the region with a distinct, narrow peak of the distribution.

In this method, we first randomly selected initial point $\boldsymbol{q}_0$ near the attractor NHA, from which the stochastic differential equations (1) is integrated numerically with the noise intensity $D = 10^{-3}$. The evolution of the system $\boldsymbol{q}(t)$ and the random force $\xi(t)$ are tracked continuously until the system drops into a small neighborhood of the given end point $\boldsymbol{q}_f$, chosen as UC1 lying on the boundary of attraction of NHA. Then this particular path and noise realization are both conserved. Repeating this process thousands of times one obtains an ensemble of trajectories starting from NHA and terminating at point $\boldsymbol{q}_f$. By sample averaging, the prehistory probability distribution can be constructed and it contains all information with respect to the evolution process of the fluctuation. We remark that the initial point $\boldsymbol{q}_0$ is arbitrary and lie within distance Δ_D of NHA, where $\Delta_D \sim \sqrt{D}$ is the characteristic diffusion amplitude about the attractor. Furthermore, since the fluctuation time is large compared with the system's relaxation time, by the time of escape the system has already "forgotten" the initial position $\boldsymbol{q}_0$. So physically the prehistory probability distribution is independent of $\boldsymbol{q}_0$.

In Fig. 4, we plot $P_h(\boldsymbol{q}, t|\boldsymbol{q}_f, t_f)$ only for last tens of seconds before fluctuating to UC1 indicated by an arrow in the figure. The parameters of system (1) used in this and the following sections are the same as those before. Evidently, the distribution for large t has sharp peaks along certain time series in $q - t$ plane. To make it more visible, this fluctuational path is plotted above in red by tracing out the ridges of the distribution. On the other hand, tracing back in time one can see that the distribution becomes irregular and unsharp. The reason will be talked about in Sec. VI. We end this section by giving time series of the escape trajectory from the above statistical analysis in Figs. 5(a) and 5(b). We also plotted the

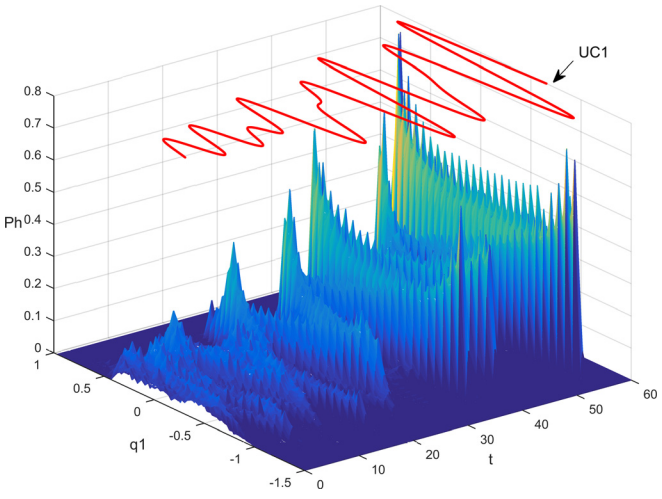

FIG. 4. Prehistory probability distribution of the escaping paths of system (1) building up by ensemble averaging thousands of trajectories. The upper red curve gives the position of ridges of the distribution which represent the optimal path.

corresponding fluctuational force during the escape by averaging the noise realizations conserved simultaneously with path realizations and performing a low-pass filtering process, with a yellow zigzag line in Fig. 5(c). We have set the instant of terminating time t_f when it fluctuates to UC1 equal to 0 in Fig. 5. The time length of the fluctuational force in Fig. 5(c) is several periods longer than that of Figs. 5(a) and 5(b) to describe the whole process of escape. An explanation on this will be given at the end of Sec. VI.

VI. ACTION PLOT

Even though the prehistory distribution shows evident and sharp peaks, it still remains necessary to verify if the fluctuational path we obtained is the optimal one, that is to say, if it attains the global minimum of the action functional $S[\boldsymbol{q}(t)]$. As discussed before, there are generally infinite many solutions of Eq. (13) which emanate from $\boldsymbol{q}_0$ and reach $\boldsymbol{q}_f$. Each of them has a corresponding action $S(\boldsymbol{q}_f)$ and provides a local minimum to the action functional. However, only those trajectories of global minimum can be observed physically in the zero noise intensity since contributions to the probability from other local minima are exponentially small. In other words, our ensemble average of fluctuational realizations should be consistent with the global minimum action trajectory, referred to as the optimal path.

The method of action plot, given by Beri *et al.*,[8] is employed here to achieve our goal. The actions of trajectories at the moment of escape manifest themselves as a function of parameters which gives a proper parametrization of the trajectories emanating from the attractor and spanning the unstable Lagrangian manifold of the Hamiltonian system. However, prior to that we need to determine a point on NHA as the initial point where trajectories can be parametrized. Recalling the work by Suso and Celso[25] which showed that, in fact, the initial condition for the most probable escape path from a NHA is uniquely determined by the primary homoclinic tangency (PHT) closest to its basin boundary. Nonhyperbolicity means that the stable and unstable manifolds of the system are tangent in the state space. If both manifolds belong to the same periodic orbit, these tangencies are homoclinic (HT). PHT is a HT where the sum of the curvatures of the stable and unstable manifolds is minimal. Their results were substantiated with the help of discrete dynamical systems such as Hénon and the Ikeda maps. Inspired by this, we turn to determine the PHT of our system.

With the algorithm proposed by Jaeger and Kantz,[26] we can locate all the homoclinic tangencies (HTs) in the entire state space containing NHA, plotted as red points in Fig. 6(a). The PHT is indicated by a green pentagram. To give a more accurate position of PHT, we select a small region of the state space, shown as the green dashed rectangle in Fig. 6(a), and present results in Fig. 6(b). The accuracy of the algorithm can be increased by taking more points in the region considered and the consequent positions of PHT do not vary obviously, ensuring its convergence to PHT. We also note that the PHT we found is requested to locate on NHA, as illustrated in Fig. 6(b). Researches investigating noise induced attractor deformations found that perturbations at a primary tangency

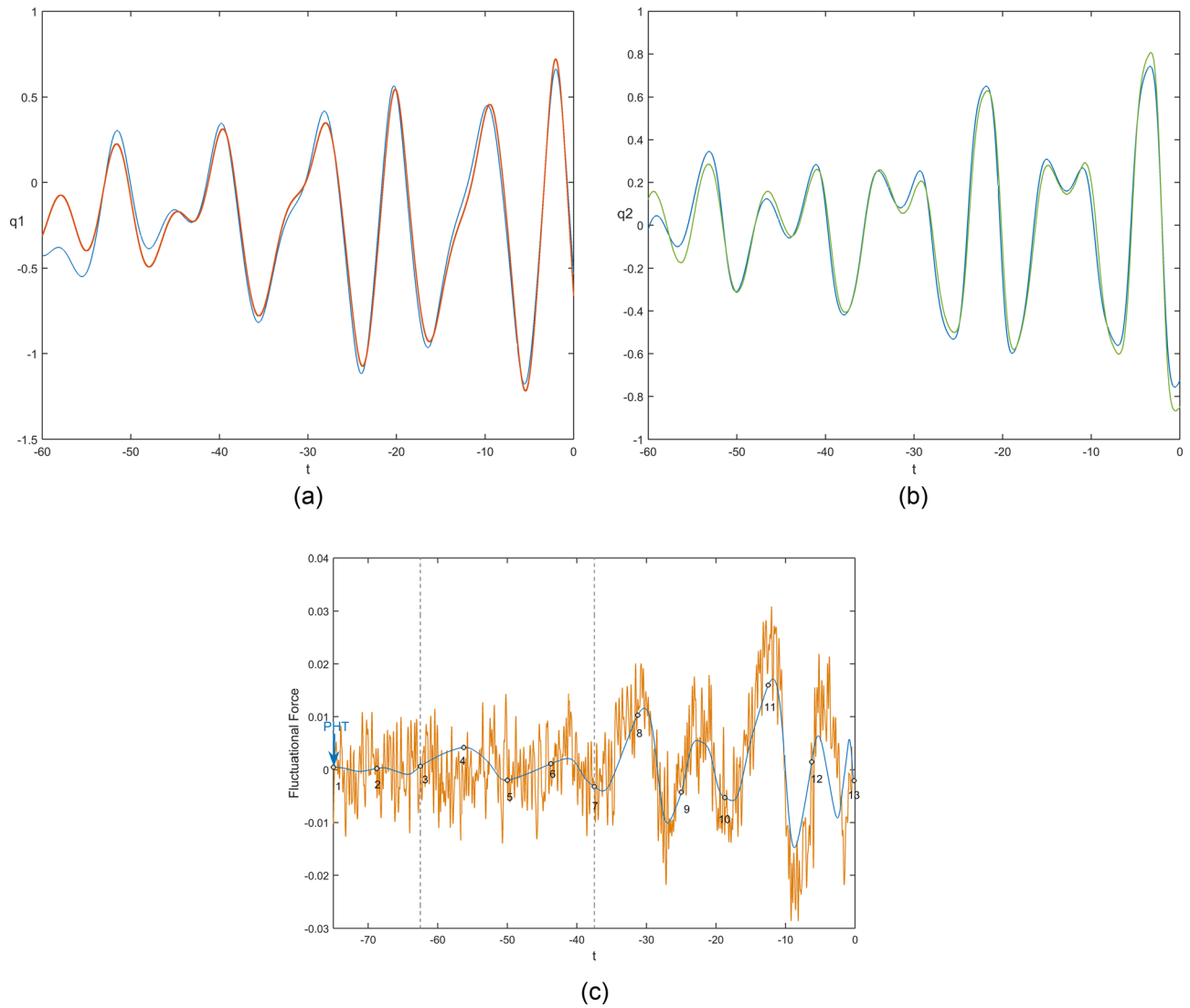

FIG. 5. (a) The escape path of q_1 component is plotted in red lines. (b) The escape path of q_1 component is in green lines. (c) The yellow zigzag line represents the fluctuational force during the escape. For comparison the optimal ones given by an action plot are also plotted here in blue. Discussions on this will be given in Section VIII.

are the most profoundly amplified both under forward and backward iterations.[31] In other words, noise causes the largest deviations at PHT and the energy to leave the attractor there is the lowest. As a consequence, it is reasonable to choose PHT on NHA as the initial condition of the escape paths.

Choosing PHT as the starting point of escape, we can parametrize the escape trajectories by taking points on a small circle (within the cell where PHT locates) centered at PHT. Thus the angular position is the parameter we use to trace out the set of escape trajectories on the unstable manifold. The action plot is then shown in Fig. 6(a). It is evident that it has a rather complicated structure composed of narrow "hills" and very sharp "peaks."[8] At the edges of hills local minima of the action are present. A zoom inside the black dashed box in Fig. 7(a) reveals almost similar structures, which is a smooth hill between two peaks at both sides. Detailed discussions about the action plot are beyond the scope of this paper and will be given elsewhere. We are now only concerned with the global minimum of the action since its corresponding escape trajectory is optimal.

We have shown the escape trajectory corresponding to the global minimum of the action in Fig. 5, in blue lines. Results by both methods display extremely good agreement, implying that the fluctuational path obtained in Sec. V is optimal to certain extent. The error between the global minimum of action plot and the action computed from statistical results is of order 10^{-4}, within the range allowed. We conclude this section by pointing out that the length of time history of Fig. 5(c) is the entire lifetime of the optimal path emanating from PHT indicated by an arrow at the beginning of the time series. Parts of the time histories of $\boldsymbol{q}(t)$ are omitted since motions for $t \leq -60$ are more chaotic, making it difficult to trace out the ridges of the prehistory probability distribution. Several escape realizations are plotted below in Fig. 8 for illustration. Their deviations from the optimal one have become evident near $t \approx -60$. This can be seen more clearly in Sec. VII.

VII. DISCUSSION ON THE MECHANISM

Now we are in a position to discuss the details of escape process and its underlying mechanism with the help of

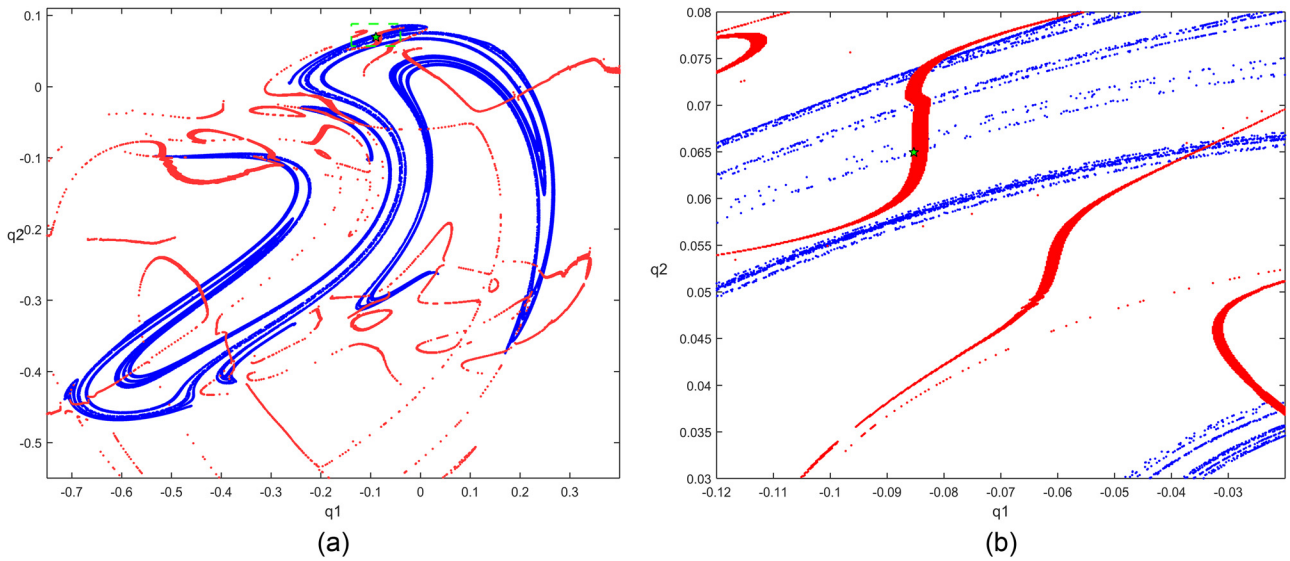

FIG. 6. (a) Homoclinic tangencies (red points) and the PHT (green pentagram) computed for a whole area containing NHA using 10^6 points distributed in the whole region. (b) Homoclinic tangencies (red points) and the PHT (green pentagram) computed only for a small region of the green dashed rectangle in (a). 2.5×10^5 points are used in this case.

optimal force of the action plot. In Fig. 5(c), we labeled 13 circles along the optimal force, each of which represents an instant of time on the same Poincare section $\omega_f t = 0 \,(\mathrm{mod}\, 2\pi)$. Then we plot these corresponding points of the optimal path in Fig. 9(a) indicated by black stars. The numbers here are identified with ones in Fig. 5(c), revealing its order of evolution.

Furthermore, to uncover the underlying mechanism we also plot the stable manifold of UC9 (SM(9)) with green dots and the unstable manifold of UC1 (UM(1)) with magenta dots in Fig. 9(a). It can be seen that UM(1) successively "passes" through UC3 and UC9 and moreover, if we plot UM(3) and UM(9) it is found that they both belong to parts of UM(1), as illustrated in Fig. 9(b). Parts of UM(1) (green) are occupied by the UM(3) (blue) and UM(9) (red). Similar situation also applies to SM(9). Thus we have the following relations:

$$\overline{UM}(1) \supseteq \overline{UM}(3) \supseteq \overline{UM}(9), \tag{14}$$

$$\overline{\mathrm{SM}}(1) \subseteq \overline{\mathrm{SM}}(3) \subseteq \overline{\mathrm{SM}}(9), \tag{15}$$

where the overbar denotes closure. Consequently, there exists a structure of heteroclinic manifold crossings between invariant manifolds of these saddle cycles. A schematic illustration of this implication is shown in Fig. 10.

With all these prepared let us turn to investigate every step of the optimal path. Point-1 is the starting point, which is the PHT on the attractor. From point-1 to point-2, the

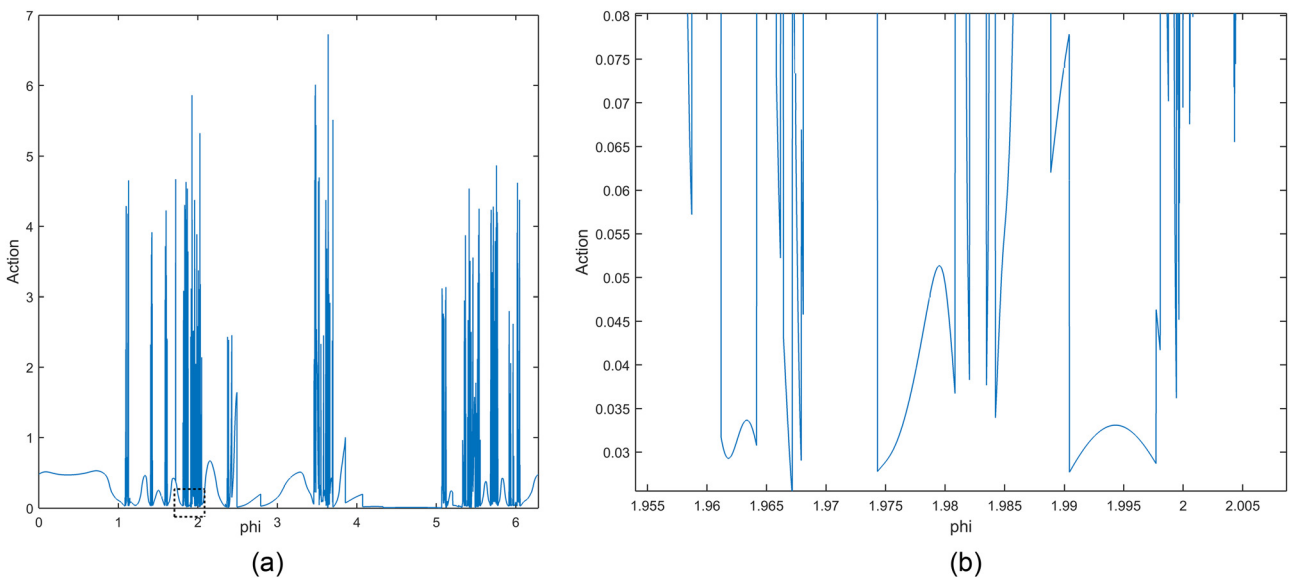

FIG. 7. (a) The action plot for our system. The x axis is the angular position to parametrize the escape trajectories, ranging from $[0, 2\pi)$. 3×10^5 points are taken in this range. (b) A local amplification of the dotted box in (a). Finer and self-similar structures are evident and infinite many local minima between each pair of peaks can be seen.

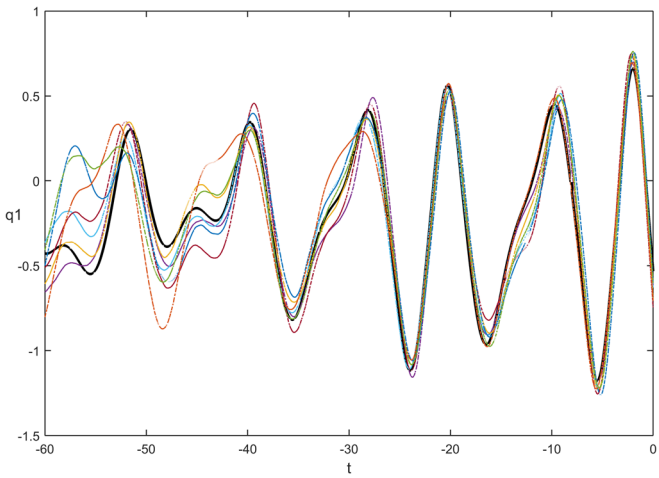

FIG. 8. The optimal path corresponding to the global minimum of the action plot (black solid line). Several escape realizations of statistical analysis (thin dashed lines in colors).

optimal force $p(t)$ remains nearly zeros as shown in Fig. 5(c), which is in accordance with Fig. 9(a) indicating that point-2 is still on NHA. During this period, the motion is dominated by deterministic regime, that is to say, chaotic regime. The motion from point-2 to point-3 is the same. This explains why an unsharp and irregular region arises in the prehistory probability distribution near $t \approx -60$ in Fig. 4.

From point-3 to point-4, $p(t)$ has a small increase, leading point-4 outside NHA but on the edge of UM(9). Subsequently, $p(t)$ undergoes a little larger change from point-4 to point-5, making point-5 located neither on NHA nor UM(9). The change of $p(t)$ from point-5 to point-6 is slightly less than that of last period and it is found that point-6 returns closely to NHA and locates near the edge of UM(9), see Fig. 9(a). However, a small immediate wiggle of

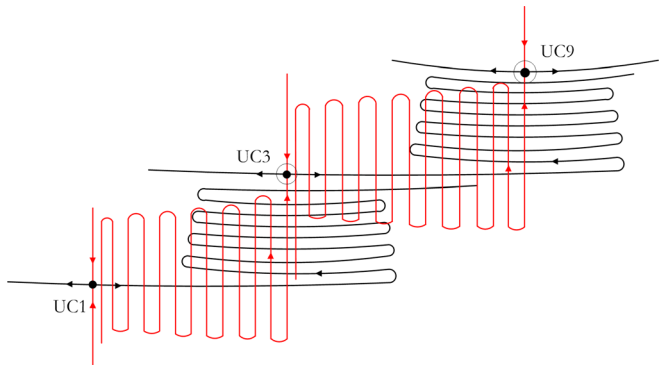

FIG. 10. A schematic illustration of the hierarchical sequence of crossings between stable and unstable manifolds of saddle cycles, demonstrating the relations of Eqs. (14) and (15).

$p(t)$ gives rise to a slightly farther distance of point-7 from NHA and UM(9).

Intriguing phenomena occur from point-7. It follows from Fig. 5(c) that $p(t)$ experiences a relatively large increase from point-7 to point-8. Taking a close look at Fig. 9(a), one can find that point-8 locates very closely to UC9 but above UC-9. Making it more precise, point-8 locates on UM(3), see Fig. 9(b). This is the first "jump" from UM(9) to UM(3), even though the position of point-8 is near UC-9.

From point-8 it seems that the optimal path moves against UM(3) until it reaches point-9 located near UC3. During this process $p(t)$ undergoes a large fluctuation and we think that a second jump from UM(3) to UM(1) may arise. However, it is quite difficult to distinguish UM(3) and UM(1) near point-9. Nevertheless, it is clear from Fig. 9(b) that point-10 does locate on UM(1) and $p(t)$ from point-9 to point-10 does to change remarkably. Therefore, we can say, that a second jump from UM(3) to UM(1) does arise between

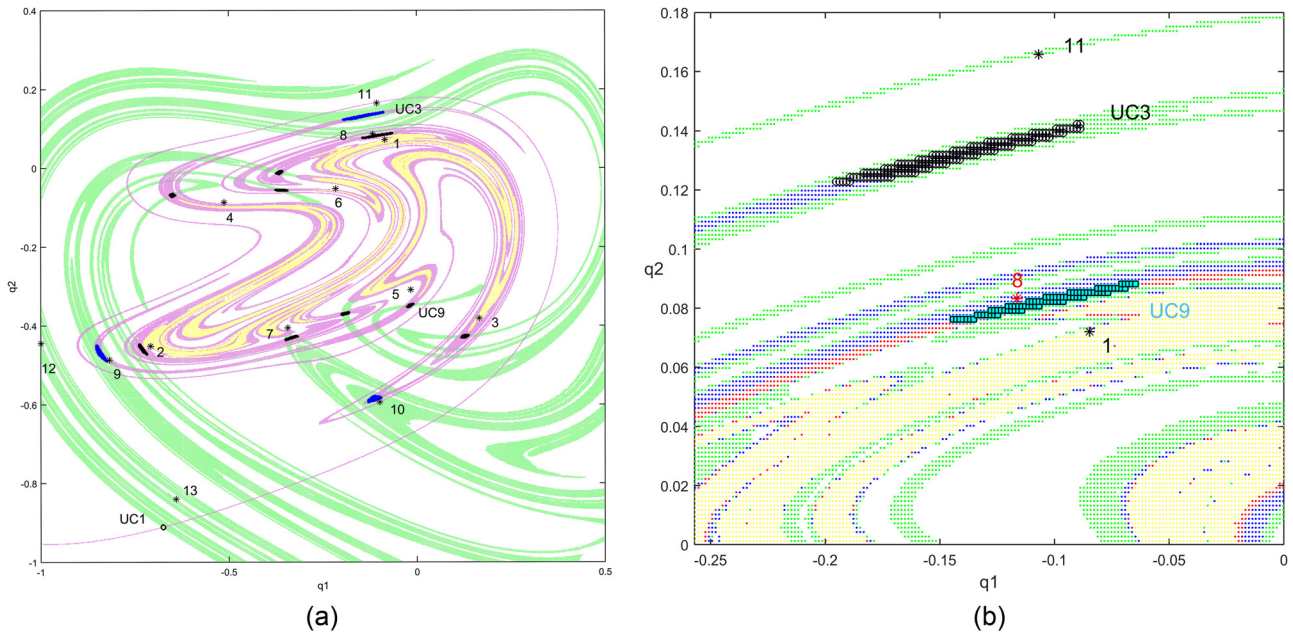

FIG. 9. (a) The optimal path and the stable manifold of UC9 (green dots) and unstable manifold of UC1 (magenta dots). Numbers indicate the order of iteration. The yellow region represents where NHA locates. (b) A local enlargement of (a) by plotting the unstable manifolds of UC1, UC3, and UC9 in green, blue, and red colors, respectively. The stars with numbers are identified with those in Fig. 9(b). It is obvious that point-8 locates in the region of blue dots, implying that it locates on UM(3). The cell state space of both (a) and (b) are 1000×1000.

point-8 and point-10 and after that $p(t)$ remains nonzero to resist the attraction.

The escape path continues its adventure from point-10 and moves to point-11 on the edge of UM(1). Afterwards, another large fluctuation in $p(t)$ emerges, resulting in the third jump from UM(1) to SM(1), i.e., point-12. The following motion should relax to noise free trajectory to UC1 in theory. We see from Fig. 5(c) that the fluctuational force oscillates nearly to zero.

Finally, we briefly discuss this hierarchical sequence of crossings between stable and unstable manifolds, first proposed by Grebogi *et al.*,[32] where they investigated basin boundary metamorphosis. Mechanism of fluctuational transitions for systems having fractal basin boundaries was studied by Silchenko *et al.*,[33] and they found similar structures of escape paths as we discussed here. In our system even if the basin boundary of NHA is not fractal, the invariant manifolds do have fractal structures and similar hierarchical sequence. UC1, created by a saddle-node bifurcation in our system, corresponds to the so-called original saddle in their work, see Fig. 1. For the parameter chosen in this paper $h = 0.143$, a homoclinic tangency of UM(1) and SM(1) has not yet occur, as shown in Fig. 2(b). However, as pointed out by Grebogi *et al.*,[32] before the parameter of their tangency, say, h^*, an infinite sequence of saddle-node bifurcations of higher periods arise as $h \to h^*$. These created stable orbits of higher periods proceed rapidly through period-doubling cascades to final crisis that destroy the stable orbits and their basins. Thus, we are convinced that the creations of UC3 and UC9 in our paper are results of saddle-node bifurcations but not period-doubling cascades, due to their odd periods. This implies UC3 and UC9 are original saddles as well as UC1. In addition, we conjecture that as $h \to h^*$, more and more unstable cycles of higher periods, like UC3 and UC9, will emerge as a result of a sequence of saddle-node bifurcations and locate closer and closer to NHA. This means the structure of hierarchical heteroclinic crossings leading to NHA is built up one "stair" by one "stair" as $h \to h^*$. However, these need further study.

VIII. CONCLUSIONS

Before summarizing our main results of this paper, a point should be clarified. It seems that such digging into extremely rare events is in contradiction with the general spirit of probability theory, which ignores events of small probability. Nevertheless, it is exactly the determination of which almost unlikely events are "more improbable" and which are "less improbable" that serves as a key to questions of what the behavior, with probability close to 1, of the process will be in an infinite time interval.[30]

In this paper, we studied the mechanism of noise induced escape from a nonhyperbolic chaotic attractor of a periodically excited nonlinear oscillator. Two saddle cycles, i.e., UC3 and UC9 are determined by GCMD method. Using the concept of prehistory probability distribution, we obtain a fluctuational escape path and the corresponding force. Both of them show extremely good agreement with the optimal ones of the action plot. Choosing the primary homoclinic tangency as the initial condition, the action plot is given and found to have complicated and self-similar structures. The global minimum of the action plot gives rise to the optimal path. Next the very details of the entire process of escape are studied step by step and roles fluctuational force plays in each period are discussed. It is found that the escape occurs through a hierarchical sequence of crossings between stable and unstable manifolds of saddle cycles, manifesting itself as a series of "jumps" from one unstable manifold to another. We conclude that it is this deterministic structure of the manifolds that determines the mechanism of fluctuational escape from NHA.

ACKNOWLEDGMENTS

This research was supported by the National Natural Science Foundation of China (Grant Nos. 11472126 and 11232007) and the Project Funded by the Priority Academic Program Development of Jiangsu Higher Education Institutions (PAPD).

[1]R. L. Kautz, Rep. Prog. Phys. **59**(59), 935–992(958) (1996).
[2]E. Arimondo, D. Hennequin, and P. Glorieux, "Noisy dynamics in optically bistable systems," in *Noise in Nonlinear Dynamical Systems* (Cambridge University Press, Cambridge and New York, 1989), Volume 3 (A90-30467 12-70), p. 119–158.
[3]P. Faure and H. Korn, Proc. Natl. Acad. Sci. **94**(12), 6506–6511 (1997).
[4]R. D. Astumian and I. Derényi, Eur. Biophys. J. **27**(5), 474–489 (1998).
[5]M. I. Dykman, P. V. Mcclintock, V. N. Smelyanski, N. D. Stein, and N. G. Stocks, Phys. Rev. Lett. **68**(18), 2718–2721 (1992).
[6]V. A. Chinarov, M. I. Dykman, and V. N. Smelyanskiy, Phys. Rev. E **47**(4), 2448–2461 (1993).
[7]M. I. Dykman and V. N. Smelyanskiy, Superlattices Microstruct. **23**(3–4), 495–504 (1998).
[8]S. Beri, R. Mannella, D. G. Luchinsky, A. N. Silchenko, and P. V. E. Mcclintock, Phys. Rev. E **72**(3 Pt 2), 036131 (2005).
[9]S. J. Einchcomb and A. J. Mckane, Phys. Rev. E **51**(4), 2974–2981 (1995).
[10]R. S. Maier and D. L. Stein, J. Stat. Phys. **83**(3–4), 291–357 (1996).
[11]A. J. Mckane, H. C. Luckock, and A. J. Bray, Phys. Rev. A **41**(2), 644–656 (1990).
[12]A. J. Bray, A. J. Mckane, and T. J. Newman, Phys. Rev. A **41**(2), 657–667 (1990).
[13]J. Gómez-Ordoñez, J. M. Casado, and M. Morillo, Phys. Rev. E **54**(2), 2125–2127 (1996).
[14]D. G. Luchinsky and P. V. Mcclintock, Nature **389**(6650), 463–466 (1997).
[15]D. G. Luchinsky, P. V. E. Mcclintock, and M. I. Dykman, Rep. Prog. Phys. **61**(8), 889–997 (1998).
[16]P. Grassberger, J. Phys. A: Math. Gen. **22**(16), 3283–3290 (1989).
[17]M. I. Dykman, M. M. Millonas, and V. N. Smelyanskiy, Phys. Lett. A **195**(1), 53–58 (1994).
[18]M. I. Dykman, D. G. Luchinsky, P. V. Mcclintock, and V. N. Smelyanskiy, Phys. Rev. Lett. **77**(26), 5229–5232 (1996).
[19]D. G. Luchinsky, R. S. Maier, R. Mannella, P. V. E. Mcclintock, and D. L. Stein, Phys. Rev. Lett. **79**(17), 3109–3112 (1997).
[20]A. J. Bray and A. J. Mckane, Phys. Rev. Lett. **62**(5), 493–496 (1989).
[21]V. S. Anishchenko, I. A. Khovanov, N. A. Khovanova, D. G. Luchinsky, and P. V. E. Mcclintock, Fluctuation Noise Lett. **1**(1), L27–L33 (2001).
[22]V. S. Anishchenko, D. G. Luchinsky, P. V. E. Mcclintock, I. A. Khovanov, and N. A. Khovanova, J. Exp. Theor. Phys. **94**(4), 821–833 (2002).
[23]D. G. Luchinski and I. A. Khovanov, JETP Lett. **69**(69), 825–830 (1999).
[24]D. G. Luchinsky, S. Beri, R. Mannella, P. V. E. Mcclintock, and I. A. Khovanov, Int. J. Bifurcation Chaos Appl. Sci. Eng. **12**(3), 583–604 (2002).
[25]S. Kraut and C. Grebogi, Phys. Rev. Lett. **92**(23), 234101 (2004).
[26]L. Jaeger and H. Kantz, Physica D **105**(1–3), 79–96 (1997).
[27]I. A. Khovanov, D. G. Luchinsky, R. Mannella, and P. V. Mcclintock, Phys. Rev. Lett. **85**(10), 2100–2103 (2000).

[28]C. S. Hsu, Int. J. Bifurcation Chaos Appl. Sci. Eng. **5**(4), 1085–1118 (1995).
[29]C. S. Hsu, *Cell-to-Cell Mapping* (Springer, New York, 1987).
[30]M. Freidlin and A. Wentzell, Probab. Theory Relat. Fields **128**(3), 441–466 (2004).
[31]M. Diestelhorst, R. Hegger, L. Jaeger, H. Kantz, and R.-P. Kapsch, Phys. Rev. Lett. **82**(11), 2274 (1999).
[32]C. Grebogi, E. Ott, and J. A. Yorke, Physica D **24**(1), 243–262 (1987).
[33]A. Silchenko, S. Beri, D. G. Luchinsky, and P. V. McClintock, Phys. Rev. E **71**(4), 046203 (2005).